CILAMCE 2017
Florianópolis - Santa Catarina - Brazil

PIEZOELECTRIC HARVESTER TOPOLOGY OPTIMIZATION USING A MULTIPARAMETER MATERIAL MODEL

Breno Vincenzo de Almeida

Renato Pavanello

brenodealmeida4@gmail.com

pava@fem.unicamp.br

University of Campinas. School of Mechanical Engineering. Department of Computational Mechanics

Cidade Universitria Zeferino Vaz - Barao Geraldo, 13083-970 , Campinas, Sao Paulo, Brazil

Abstract. *During the past decade, methods of reusing environmental vibration energy have been developed, to transform it in useful, electric, energy and store it in batteries or capacitors, especially due to the reduced power requirement of electronic devices, such as cellphones and global positioning systems. This could also contribute to the environment, since batteries would be less used, thus diminishing their chemical waste, as well as decreasing maintenance and energy costs. One of the methods to reach these goals is to increase the energy efficiency of electronic devices, by reusing ambient vibrational waste energy in useful energy, in other words, harvesting it and the piezoelectric harvester is one of the most interesting vibration-to-energy conversion mechanisms. In this article a piezoelectric harvesting device is modelled as a bimorph cantilever beam, with an intermediate metallic substrate, under plain strain hypothesis. The design of the piezoelectric material of the harvester is then structurally optimized using the proposed multiparameter Bidirectional Evolutionary Structural Optimization (BESO) method to minimize an inverse conversion factor. Different penalization factors, one for each physical property of the piezoelectric material, are chosen in order to find a better convergence for the algorithm and to make more stable. Numerical results for the multiparameter analysis are displayed and analysed, in order to study the influence of the harvester's geometry and its different substrate materials on the conversion factor.*

Keywords: *piezoelectric, harvester, structural optimization*

1 INTRODUCTION

Piezoelectric materials have an intrinsic coupling effect between strain energy and electric displacement. When a mechanical force is applied to a piezoelectric ceramic, an electric field proportional to the applied strain will appear. The phenomenon described is called the direct piezoelectric effect and was discovered by the Curie brothers - Pierre and Jacques Curie - in 1880. Lippmann (1881) then used thermodynamic principles to obtain the inverse piezoelectric effect, in which a piezoelectric material deforms when subjected to an applied electric field and which was empirically proven by the Curie brothers in 1881. During the first half of the XX century, various naturally occurring piezoelectric materials were discovered, such as sodium potassium tartrate (Rochelle salt), quartz, among others, but none of which had a sufficient electromechanical coupling effect to be useful for engineering applications. Piezoelectric ceramics were then developed during the second half of the XX century to fix this issue. Nowadays, the most commonly used piezoceramic is lead zirconate titanate, PZT (Erturk & Inman, 2011).

During the initial developments of piezoelectric energy harvesters, many model simplifications were made, due to the higher complexities involved in dealing with multi-physical phenomena. Thus, the first harvester models were generally of clamped beams with lumped parameters, which was considerably advantageous, since the electrical part of the problem could be more easily separated in the lumped parameters, such as a capacitor due to the inherent piezoelectric capacitance and a resistance, and the main difficulty would be to find the lumped parameters for the mechanical aspect of the system, only then considering the relationship between the two different energies by means of the constitutive coupling piezoelectric effects (Roundy & Wright, 2004). Although the lumped parameter models could serve as a useful first approximation to piezoelectric phenomena, they are not considerably precise, due to being limited by one mode of vibration and not having the inherent characteristic of a coupled system, such as vibration modes and strain distribution. Another important aspect to consider is that these models generally do not take the distributed mass of the beam into account, which can effect the result of optimization problems due to the different modes of vibration (Erturk & Inman, 2011).

A discrete formulation was then developed using the Rayleigh-Ritz method (Young W. Kwon, 2000), based on an Euler-Bernoulli beam model (Sodano et al., 2004; Dutoit et al., 2005). With the Rayleigh-Ritz method one can obtain a spatially discrete model from a distributed parameter system (continuous system), finding a finite number of degrees of freedom. It is generally less computationally efficient than an analytical solution (if one exists). To find analytical solutions instead, one can use the modes of vibration obtained by the Euler-Bernoulli beam model and combine it with the piezoelectric constitutive equations with which one obtains the electric displacements to find the relationship between the electric output and each mode of vibration. Such solutions were developed and empirically tested by Erturk & Inman (2011), which converged to the Rayleigh-Ritz formulation.

In parallel to the developments regarding modelling of piezoelectric phenomena, close to the end of the XX century, with the advances on computation, Finite Element Analysis (FEA) implementations were becoming increasingly more sophisticated and structural optimization techniques to continuum structures were gaining popularity, such as the Solid Isotropic Material with Penalization (SIMP) method (Bendsoe & Sigmund, 2013) and the Evolutionary Structural

Optimization (ESO) method (Steven & Xie, 2014). These advances were amply applied especially to solve compliance minimization and natural frequency maximization related problems, not only for large structures but also at the micro-scale (Huang & Xie, 2010).

Structural optimization techniques have also been applied to numerous different multiphysical problems, such as: frequency response of fluid-structure systems (Vicente et al., 2015), automotive muffler acoustic topology optimization (Azevedo et al., 2016) and frequency maximization problems for acoustic-structure interaction (Picelli et al., 2015), among others. More interestingly for this paper, various articles have been written for the topology optimization of piezoelectric materials and its applications: Sigmund et al. (1998) optimized the design of 1-3 piezocomposites for piezoelectric transducers, as did Silva et al. (1999) but with a homogenization approach and Donoso & Sigmund (2008) considered optimal design problems for active damping. Furthermore, advances were made in the area of energy harvesting devices: Kiyono et al. (2016) optimized a piezoelectric harvester modelled with a multilayered shell element, Zheng et al. (2008) focused on optimizing a three-dimensional piezoelectric harvester subjected to static loading conditions using a FE mesh and Noh & Yoon (2012) further developed this by considering dynamic as well as static loads and using different penalization factors for each of the piezoelectric material's physical properties. Most of these articles used the SIMP method for the optimization problem.

In this paper a different approach is taken for the piezoelectric harvester topology optimization. The harvester is modelled as a bimorph two dimensional beam under plain strain hypothesis, as a section of a three dimensional beam, as shown in Fig. 1. The beam is composed of two piezoelectric layers of opposing polarities and an intermediate metallic substrate.

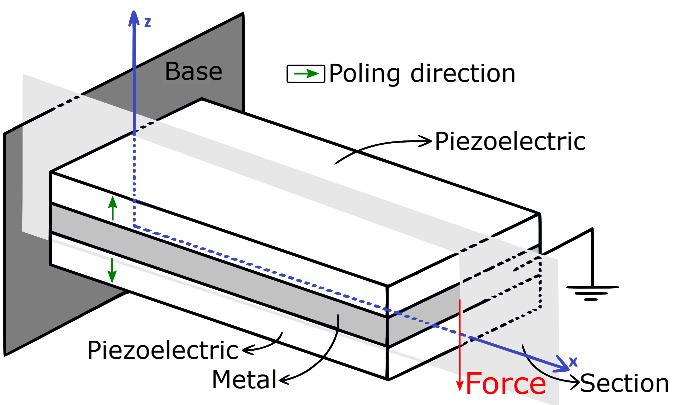

Figure 1: Piezoelectric harvester model

The BESO method is then used to optimize the topology of the piezoelectric material of the harvester, considering a static load on the free end of the beam and a fix topology for the metallic substrate. The sensitivities of a minimization problem are derived and different penalization parameters are used for each of the piezoelectric material's stiffness (Noh & Yoon, 2012) in order to find a better convergence. Numerical results are then displayed and the influence of the harvester's geometry and the substrate's material on the objective function are studied.

2 MODEL FORMULATION

Using index notation, the stress-charge form of the piezoelectric constitutive equations is shown in Eq. (1).

$$
\begin{aligned}
T_{ij} &= c^{E}_{ijkl} S_{kl} - e_{kij} E_k \\
D_i &= e_{ikl} S_{kl} + \varepsilon^{S}_{ij} E_k
\end{aligned}
\tag{1}
$$

In Eq. (1) T, S, D and E are the stress, strain, electric displacement and electric field, respectively (IEEE, 1988). Furthermore, c_{ijkl} is the elastic tensor for a null or constant electric field, e_{ikl} is the piezoelectric coupling tensor and ε_{ij} is the dielectric permittivity tensor for null or constant strain.

Considering plain strain hypothesis (ϵ_{22},ϵ_{12},$\epsilon_{32} = 0$) by modelling the harvester as the section shown in Fig. 1, Eq. (1) can be simplified to (Rajapakse, 1997):

$$
\begin{aligned}
T_{11} &= c_{11} S_{11} + c_{11} S_{33} - e_{31} E_3 \\
T_{33} &= c_{13} S_{11} + c_{33} S_{33} - e_{33} E_3 \\
T_{13} &= 2 c_{44} S_{13} - e_{15} E_1 \\
D_1 &= 2 e_{15} S_{13} + \varepsilon_{11} E_1 \\
D_3 &= e_{31} S_{11} + e_{33} \epsilon_{33} + \varepsilon_{33} E_3
\end{aligned}
\tag{2}
$$

Equation (2) is written considering that the piezoelectric layers have reverse poling directions aligned to the z axis.

The boundary conditions are defined as below.

$$
\begin{aligned}
T_{r_i} &= T^{*}_{r_i} \quad \text{or} \quad u_i = u^{*}_i \quad \text{in} \quad \Gamma, \quad i = 1,3 \\
D_i n_i &= -Q^{*} \quad \text{or} \quad \phi = \phi^{*} \quad \text{in} \quad \Gamma, \quad i = 1,3
\end{aligned}
\tag{3}
$$

In Eq. (3), Γ is the boundary, T_{r_i} and n_i are the traction and unit vector component perpendicular to Γ in direction i, respectively, and e $T^{*}_{r_i}$, u^{*}_i, Q^{*} and ϕ^{*} are the given values for traction and displacement in direction i, surface electric charge and electric potential, respectively.

The compact form of Eq. (1) is:

$$
\begin{aligned}
\mathbf{T} &= \mathbf{c}^{E} \mathbf{S} - \boldsymbol{e} \mathbf{E} \\
\mathbf{D} &= \mathbf{e}^{T} \mathbf{S} + \boldsymbol{\varepsilon}^{S} \mathbf{E}
\end{aligned}
\tag{4}
$$

Under FE formulation the element strain and electric field can be represented with respects to its nodal displacements $\mathbf{u}^e$ and the nodal electric potential $\boldsymbol{\phi}^e$ as shown below.

$$
\begin{aligned}
\mathbf{S}^e &= \mathbf{B}_u \mathbf{u}^e \\
\mathbf{E}^e &= \mathbf{B}_\phi \boldsymbol{\phi}^e
\end{aligned}
\tag{5}
$$

In Eq. (5), $\mathbf{B}_u$ and $\mathbf{B}_\phi$ are the first order derivatives of the shape functions used to interpolate the displacement and electric potential fields, respectively.

Substitution of Eq. (5) in Eq. (4) results in the element wise stress and electric displacement:

$$\begin{aligned}\mathbf{T}^e &= \mathbf{c}^E\mathbf{B}_u\mathbf{u}^e - \boldsymbol{e}\mathbf{B}_\phi\boldsymbol{\phi}^e \\ \mathbf{D}^e &= \mathbf{e}^T\mathbf{B}_u\mathbf{u}^e + \boldsymbol{\varepsilon}^S\mathbf{B}_\phi\boldsymbol{\phi}^e\end{aligned} \tag{6}$$

Equations (3) to (6) can then be used to determine the FE equilibrium equations for piezoelectric elements and static loading condtions (Bendigeri et al., 2011; Zheng et al., 2008; Noh & Yoon, 2012):

$$\begin{bmatrix}\mathbf{K}^e_{uu} & \mathbf{K}^{eT}_{\phi u} \\ \mathbf{K}^e_{\phi u} & -\mathbf{K}^e_{\phi\phi}\end{bmatrix}\begin{bmatrix}\mathbf{u}^e \\ \boldsymbol{\phi}^e\end{bmatrix} = \begin{bmatrix}\mathbf{F}^e \\ \mathbf{Q}^e\end{bmatrix} \tag{7}$$

In Eq. (7), $\mathbf{K}^e_{uu}$, $\mathbf{K}^e_{u\phi}$ and $\mathbf{K}^e_{\phi\phi}$ are the element mechanical stiffness, piezoelectric coupling and dielectric permittivity matrices, and $\mathbf{F}^e$ and $\mathbf{Q}^e$ are the applied nodal force and charge vectors, respectively. The stiffness matrices are calculated through the following integrations:

$$\begin{aligned}\mathbf{K}^e_{uu} &= \int_{\Gamma^e}\mathbf{B}_u^T\mathbf{c}^E\mathbf{B}_u d\Gamma^e \\ \mathbf{K}^e_{\phi u} &= \int_{\Gamma^e}\mathbf{B}_\phi^T\mathbf{e}^T\mathbf{B}_u d\Gamma^e \\ \mathbf{K}^e_{\phi\phi} &= \int_{\Gamma^e}\mathbf{B}_\phi^T\boldsymbol{\varepsilon}^S\mathbf{B}_\phi d\Gamma^e\end{aligned} \tag{8}$$

To solve the global FE model, the stiffness of every elements are assembled to the global system, and the equation below is obtained.

$$\begin{bmatrix}\mathbf{K}_{uu} & \mathbf{K}^{T}_{\phi u} \\ \mathbf{K}_{\phi u} & -\mathbf{K}_{\phi\phi}\end{bmatrix}\begin{bmatrix}\mathbf{u} \\ \boldsymbol{\phi}\end{bmatrix} = \begin{bmatrix}\mathbf{F} \\ \mathbf{Q}\end{bmatrix} \tag{9}$$

In this paper the main piezoelectric material used is PZT-4, which has the following property matrices, considering that it is polarized along the z-direction, according to the Institute of Electrical and Electronics Engineers' (IEEE, 1988) standard:

$$\mathbf{e} = \begin{bmatrix} 0 & 0 & -5.2 \\ 0 & 0 & -5.2 \\ 0 & 0 & 15.1 \\ 0 & 12.7 & 0 \\ 12.7 & 0 & 0 \\ 0 & 0 & 0 \end{bmatrix} C/m^2 \tag{10}$$

$$\mathbf{c^E} = \begin{bmatrix} 1.39 & 0.778 & 0.743 & 0 & 0 & 0 \\ 0.77 & 1.39 & 0.743 & 0 & 0 & 0 \\ 0.743 & 0.743 & 1.15 & 0 & 0 & 0 \\ 0 & 0 & 0 & 0.256 & 0 & 0 \\ 0 & 0 & 0 & 0 & 0.256 & 0 \\ 0 & 0 & 0 & 0 & 0 & 0.306 \end{bmatrix} \cdot 10^2 GPa \tag{11}$$

$$\boldsymbol{\varepsilon}^{\boldsymbol{S}} = \begin{bmatrix} 6.45 & 0 & 0 \\ 0 & 6.45 & 0 \\ 0 & 0 & 5.62 \end{bmatrix} nF/m \tag{12}$$

3 OPTIMIZATION PROBLEM

In this paper, the BESO method is used to find the optimal harvester topology. The soft-kill BESO method is used, in which a material interpolation scheme with penalization for intermediate densities is considered for the three stiffnessess shown in Eq. (8). The main advantages of using this topology optimization method are that it is a sensitivity base method, it uses discrete variables and is relatively simple to implement. Mesh dependency and checkerboard pattern are avoided by the application of a filter in each iteration (Huang & Xie, 2010).

A flow chart of the soft-kill BESO optimization procedure is shown in Fig. 2. The first step is to determine the initial topology, the properties of each material and the boundary constraints. A loop is then initialized, where a FE analysis of the harvester is done to obtain the nodal displacements and nodal electric potentials. Next a sensitivity calculation is performed, to determine which elements should be solid and which should become void to minimize the objective function. A filter is then applied, to avoid mesh dependency and checkerboard pattern. The topology is then reconfigured according to the sensitivity analysis.

In this paper the design domain is considered to be only the piezoelectric elements. Thus, the applied filter does not take the elements of the metallic substrate into account. Furthermore, in this paper the initial volume is compose of 100% solid elements. The loop continues until the final volume is reached and the stopping criterion is met. The stopping criterion is determined by the last 10 iterations objective functions' variability, which has to be lower than a very small value (eg. 10^{-6}).

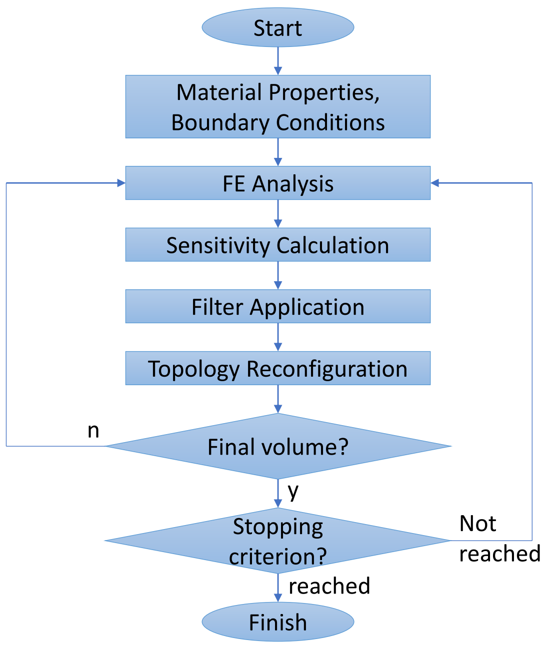

Figure 2: BESO flow chart

The following minimization problem is solved for the piezoelectric harvester's optimization algorithm (Zheng et al., 2008):

$$
\begin{aligned}
\text{minimize} \quad & \zeta = 1 + \frac{\Pi^S}{\Pi^E} \\
\text{subject to} \quad & V^* - \sum_{i=1}^{N} V_i x_i = 0 \\
& x_i = x_{min} \text{ ou } x_i = 1 \\
& i = 1, \ldots, \text{number of elements}
\end{aligned}
\tag{13}
$$

In Eq. (13), ζ is the inverse conversion factor of the electric energy Π^E divided by the work of the applied force. This work is equal to the sum of the electric and the mechanical (or strain) energy Π^S.

The element sensitivities α_i are obtained by the derivative of the objective function with respects to the i-th element's density x_i:

$$
\alpha_i = \frac{\partial \zeta}{\partial x_i} = \frac{1}{\Pi^E}\frac{\partial \Pi^S}{\partial x_i} - \frac{\Pi^S}{(\Pi^E)^2}\frac{\partial \Pi^E}{\partial x_i}
\tag{14}
$$

The derivative of the strain energy with respects to the i-th element's density is obtained by applying the adjoint method (Zheng et al., 2008):

$$
\Pi^S = \frac{1}{2}\mathbf{u}^T\mathbf{K}_{uu}\mathbf{u} + \boldsymbol{\lambda}_1^T\left(\mathbf{K}_{uu}\mathbf{u} + \mathbf{K}_{u\phi}\boldsymbol{\phi} - \mathbf{F}\right) + \boldsymbol{\mu}_1^T\left(\mathbf{K}_{\phi u}\mathbf{u} - \mathbf{K}_{\phi\phi}\boldsymbol{\phi}\right)
\tag{15}
$$

In Eq. (15), $\boldsymbol{\lambda}_1$ and $\boldsymbol{\mu}_1$ are the adjoint terms. Notice that $\mathbf{Q} = \mathbf{0}$, since no external charge is applied to the harvester.

Thus, the derivative becomes:

$$
\begin{aligned}
\frac{\partial \Pi^S}{\partial x_i} = & \left(\mathbf{u}^T\mathbf{K}_{uu} + \boldsymbol{\lambda}_1^T\mathbf{K}_{uu} + \boldsymbol{\mu}_1\mathbf{K}_{\phi u}\right)\frac{\partial \mathbf{u}}{\partial x_i} + \left(\boldsymbol{\lambda}_1^T\mathbf{K}_{u\phi} - \boldsymbol{\mu}_1^T\mathbf{K}_{\phi\phi}\right)\frac{\partial \boldsymbol{\phi}}{\partial x_i} \\
& + \frac{1}{2}\mathbf{u}^T\frac{\partial \mathbf{K}_{uu}}{\partial x_i}\mathbf{u} + \frac{\partial \boldsymbol{\lambda}_1^T}{\partial x_i}\left(\mathbf{K}_{uu}\mathbf{u} + \mathbf{K}_{u\phi}\boldsymbol{\phi} - \mathbf{F}\right) + \frac{\partial \boldsymbol{\mu}_1^T}{\partial x_i}\left(\mathbf{K}_{\phi u}\mathbf{u} - \mathbf{K}_{\phi\phi}\boldsymbol{\phi}\right) \\
& + \boldsymbol{\lambda}_1^T\frac{\partial \mathbf{K}_{uu}}{\partial x_i}\mathbf{u} + \boldsymbol{\lambda}_1^T\frac{\partial \mathbf{K}_{u\phi}}{\partial x_i}\boldsymbol{\phi} + \boldsymbol{\mu}_1^T\frac{\partial \mathbf{K}_{\phi u}}{\partial x_i}\mathbf{u} - \boldsymbol{\mu}_1^T\frac{\partial \mathbf{K}_{\phi\phi}}{\partial x_i}\boldsymbol{\phi} + \boldsymbol{\lambda}_1^T\frac{\partial \mathbf{F}}{\partial x_i}
\end{aligned}
\tag{16}
$$

In Eq. (16), the external force $\mathbf{F}$ is constant with respects to x_i, thus its derivative is null, and the terms multiplied by $\partial\boldsymbol{\lambda}_1^T/\partial x_i$ and by $\partial\boldsymbol{\lambda}_1^T/\partial x_i$ are also null, due to the equilibrium Eq. (9) and because $\mathbf{Q} = \mathbf{0}$. Furthermore, using the adjoint method, the terms multiplying $\partial\mathbf{u}/\partial x_i$ and by $\partial\boldsymbol{\phi}/\partial x_i$ are equal to zero, thus the following linear system of equations is obtained:

$$
\begin{bmatrix} \mathbf{K}_{uu} & \mathbf{K}_{u\phi} \\ \mathbf{K}_{\phi u} & -\mathbf{K}_{\phi\phi} \end{bmatrix}
\begin{Bmatrix} \boldsymbol{\lambda}_1 \\ \boldsymbol{\mu}_1 \end{Bmatrix}
=
\begin{Bmatrix} -\mathbf{K}_{uu}\mathbf{u} \\ \mathbf{0} \end{Bmatrix}
\tag{17}
$$

After calculating the adjoint terms, their values can then be substituted in Eq. (16) and the complete sensitivity for the strain energy can be calculated:

$$
\frac{\partial \Pi^S}{\partial x_i} = \left(\frac{1}{2}\mathbf{u}^T + \boldsymbol{\lambda}_1^T\right)\frac{\partial \mathbf{K}_{uu}}{\partial x_i}\mathbf{u} + \boldsymbol{\lambda}_1^T\frac{\partial \mathbf{K}_{u\phi}}{\partial x_i}\boldsymbol{\phi} + \boldsymbol{\mu}_1^T\frac{\partial \mathbf{K}_{\phi u}}{\partial x_i}\mathbf{u} - \boldsymbol{\mu}_1^T\frac{\partial \mathbf{K}_{\phi\phi}}{\partial x_i}\boldsymbol{\phi}
\tag{18}
$$

Analogously to equations (17) and (18), to find the adjoint terms $\boldsymbol{\lambda}_2$ and $\boldsymbol{\mu}_2$ for the sensitivity of the electric energy the following linear system is solved:

$$\begin{bmatrix} \mathbf{K}_{uu} & \mathbf{K}_{u\phi} \\ \mathbf{K}_{\phi u} & -\mathbf{K}_{\phi\phi} \end{bmatrix} \begin{Bmatrix} \boldsymbol{\lambda}_2 \\ \boldsymbol{\mu}_2 \end{Bmatrix} = \begin{Bmatrix} \mathbf{0} \\ -\mathbf{K}_{\phi\phi}\boldsymbol{\phi} \end{Bmatrix} \tag{19}$$

With the adjoint terms, the sensitivity of the electric energy with respects to the i-th element's density:

$$\frac{\partial \Pi^E}{\partial x_i} = \frac{1}{2}\boldsymbol{\phi}^T \frac{\partial \mathbf{K}_{\phi\phi}}{\partial x_i}\boldsymbol{\phi} + \boldsymbol{\lambda}_2^T \frac{\partial \mathbf{K}_{uu}}{\partial x_i}\mathbf{u} + \boldsymbol{\lambda}_2^T \frac{\partial \mathbf{K}_{u\phi}}{\partial x_i}\boldsymbol{\phi} + \boldsymbol{\mu}_2^T \frac{\partial \mathbf{K}_{\phi u}}{\partial x_i}\mathbf{u} - \boldsymbol{\mu}_2^T \frac{\partial \mathbf{K}_{\phi\phi}}{\partial x_i}\boldsymbol{\phi} \tag{20}$$

The last terms that need to be defined to determine the sensitivities in Eqs. (18) and (20) depend on the mathematical material model used to find the relationship between each of the piezoelectric material's properties with the element's density x_i. A material interpolation scheme similar to the SIMP method is used, but considering one penalization value for each of the stiffness components, as done by Noh & Yoon (2012). Thus, the stiffness matrices of each element is:

$$\mathbf{K}^e_{uu} = x^{p_1}\mathbf{K}^e_{uu} \qquad \mathbf{K}^e_{\phi u} = x^{p_2}\mathbf{K}^e_{\phi u} \qquad \mathbf{K}^e_{\phi\phi} = x^{p_3}\mathbf{K}^e_{\phi\phi} \tag{21}$$

In Eq. (21), $0 < x \leq 1$ and p_1, p_2 and p_3 are the penalization factors for the mechanical, piezoelectric and electrical stiffness matrices, respectively. They are introduced in order to find a better convergence for the optimization algorithm.

In order to further stabilize the algorithm, extra weight factors w_S e w_E were used in Eq. (14) for the mechanical and electrical contributions to the sensitivity, respectively:

$$\alpha_i = w_S \frac{1}{\Pi^E}\frac{\partial \Pi^S}{\partial x_i} - w_E \frac{\Pi^S}{(\Pi^E)^2}\frac{\partial \Pi^E}{\partial x_i} \tag{22}$$

In this context a multiparameter (p_1, p_2, p_3, w_S and w_E) algorithm has been proposed, implemented and tested. In the next sections, analyses of the influence of the penalization factors, the harvester's geometry and the material properties are presented.

4 PENALIZATION FACTOR ANALYSIS

The analyses presented in this and the next two sections consider a piezoelectric harvester illustrated in Fig. 3, which shows the design of the piezoelectric energy harvester, with the poling directions, the applied force F, the harvester's length L, its thickness H and the substrate thickness, equal to a percentage of the total thickness βH, where $0 < \beta < 1$.

4.1 Example 1: Initial analysis

For a first example, the soft-kill BESO algorithm explained in the previous sections were applied for a piezoelectric harvester with the piezoelectric material made of PZT-4 and the metallic substrate made of steel with an elasticity constant of $200GPa$ and a Poisson coefficient

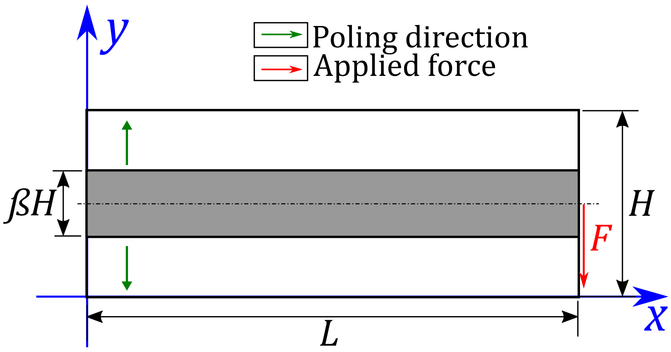

Figure 3: Piezoelectric harvester two dimensional section

of 0.29. The geometric properties are $L = 100mm$, $H = 40mm$ and $\beta = 20\%$ ($\beta H = 8mm$). The left-hand side of Fig. 3 is the harvester's base, which is clamped, and a downward force of $100N$ is applied on the free end (right-hand side of the beam in the same figure).

As previously mentioned, the design domain consists solely on the piezoelectric layers. The optimization procedure was done for a 120 by 60 element mesh (total of 7200 elements). The target volume of the design domain was 55% of the initial volume. The evolutionary ratio ER was 2%, the density value for the void elements was 1% and the maximum addition ratio AR was 1%. Furthermore, the filter had a radius of 20% of the beam's thickness. The results of the optimization are shown in Fig. 4.

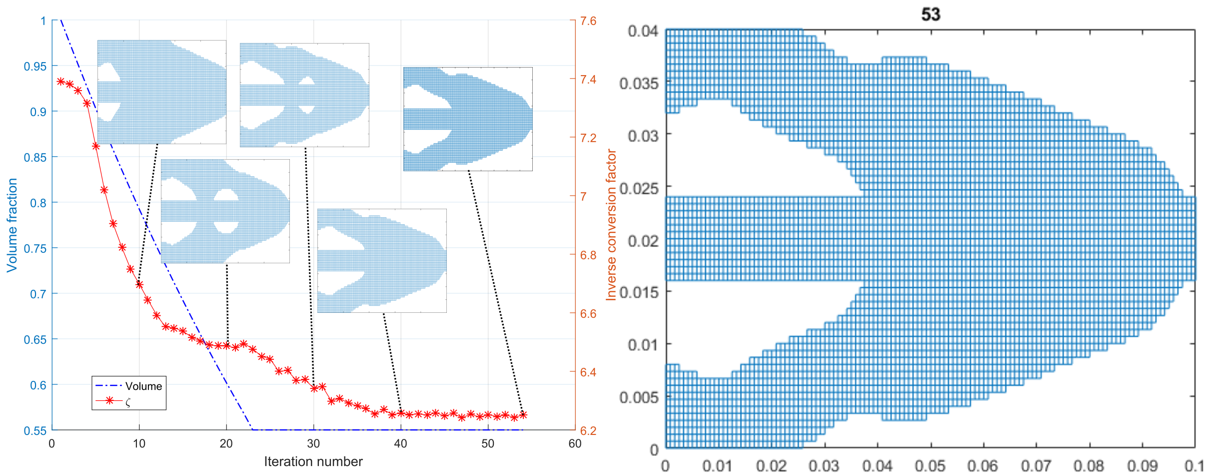

(a) Convergence curve **(b) Final topology**

Figure 4: Topology optimization results for the piezoelectric harvester described in section 4

To find the results shown in Fig. 4, the penalization factors were chosen as $p_1 = 3$, $p_2 = 2$ and $p_3 = 1$ and the sensitivity weight factors were $w_S = 60\%$ and $w_E = 40\%$.

The convergence curve shown in orange in Fig. 4a shows a relatively smooth convergence. The initial inverse conversion factor was 7.39 and was minimized to 6.25, which corresponds to a 15.42% reduction of the objective function.

4.2 Example 2: Penalization factor analysis

In order to study the effects of the penalization factors in more detail, several different combinations of the factors were chosen, with all of the other parameters kept the same as in Example 1, and the convergence curves are shown in Fig. 5a while the four best results have their respective final topologies displayed in Fig. 5b. The penalization factor combinations will be written hereafter as $[p_1, p_2, p_3]$.

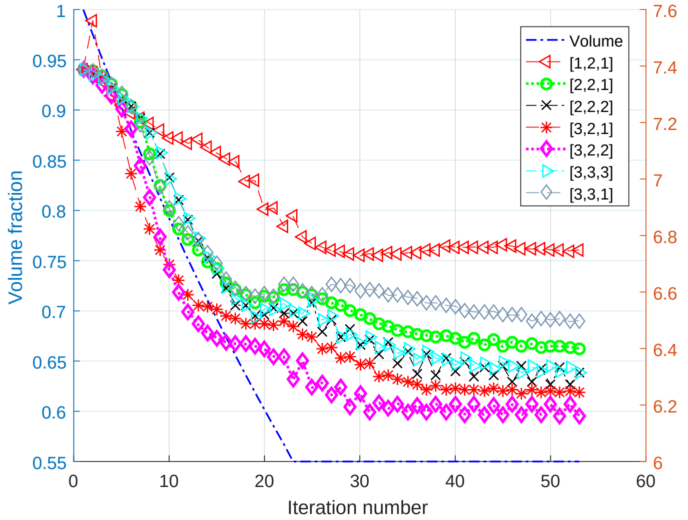

(a) Convergence curve

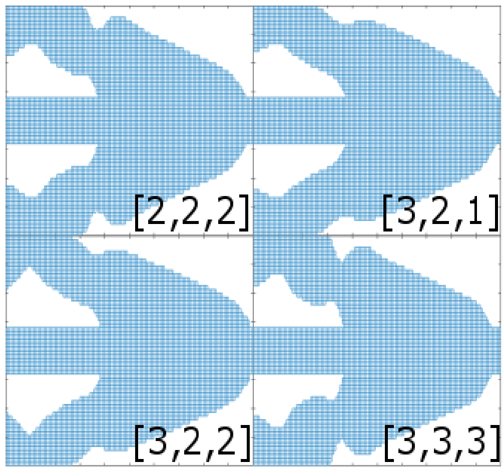

(b) Final topologies for the smallest objective functions

Figure 5: Topology optimization results for the piezoelectric harvester described in section 4 with the penalization factors shown in Fig.'s 5a legend

From Fig. 5a, it is notable that the inverse conversion factor tends to better minimized when the mechanical stiffness' penalization factor p_1 tends to 3. This is consistent with the fact that such a value is recommended when performing compliance minimization optimizations for two dimensional problems (Bendsoe & Sigmund, 2013; Huang & Xie, 2010). Moreover, after testing several other different penalization factor combinations than shown in Fig. 5, the best values for p_2 and p_1 were found to be 2 and 1, respectively. This may contradict the fact that the smallest inverse conversion factor in Fig. 5a was for $[3, 2, 2]$, but notice that, although it was smaller than for $[3, 2, 1]$, the objective function curve was less stable.

A parameter sweep was done to determine the best sensitivity weight factors and for the geometry used in Examples 1 and 2 and the best results were achieved for the values of $w_S = 60\%$ and $w_E = 40\%$.

5 HARVESTER GEOMETRIC ANALYSIS

In section 4, Examples 1 and 2 were done using the same geometric properties and one of the best optimization results was for the penalization factor combination $[3, 2, 1]$. In this section, this penalization combination will be used, but the effects of the geometric properties of the piezoelectric harvester will be analysed.

5.1 Example 3: Harvester total thickness H analysis

Three different length to thickness ratios are chosen to determined their effect on the objective function and on the algorithm's convergence. The length is fixed to $L = 100mm$. The thicknesses analysed are $H = 20mm$, $H = 40mm$ and $H = 60mm$. The other optimization parameters are $ER = 1\%$, $AR = 0.5\%$, $x_{min} = 1\%$, $w_S = 60\%$ and $w_E = 40\%$. The substrate's thickness is for $\beta = 20\%$ in all instances, the mesh is 250 by 50 elements and the filter radius is 40% of the beams total thickness. Figure 6 shows the results for this example.

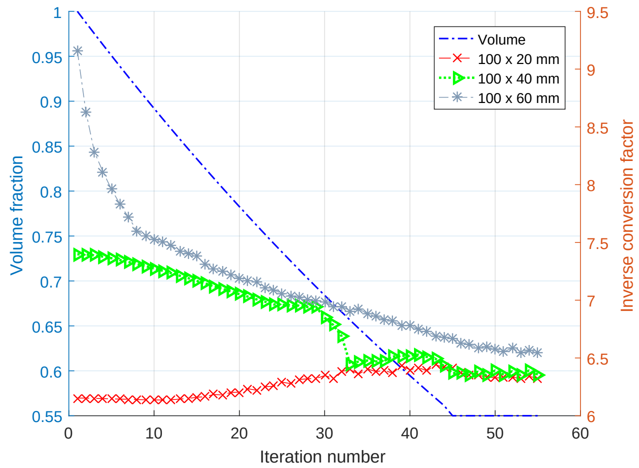

(a) Convergence curve

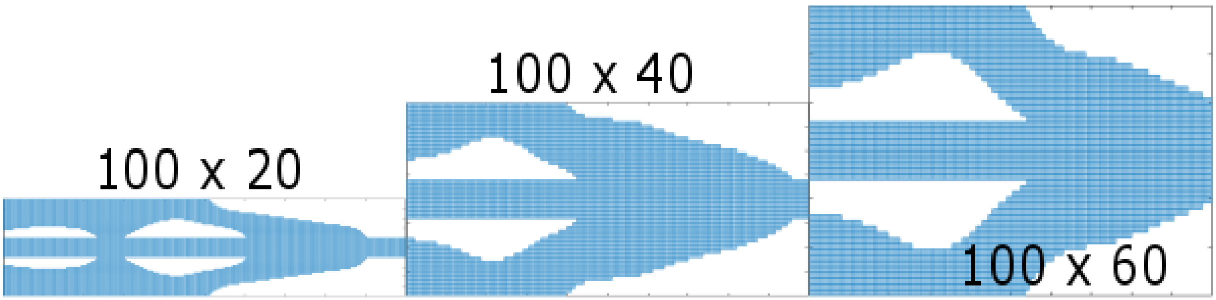

(b) Final topologies for different thicknesses

Figure 6: Topology optimization results for the piezoelectric harvester with different thicknesses

As can be seen in Fig. 6a, and through the optimization code, the objective function decreases in 25.5% for the $60mm$ thick beam and 14.1% for the $40mm$ thick beam, while it increases 2.8% for the $20mm$ thick beam. One can conclude that, on one hand, the thicker the beam, the greater the percentile minimization of the objective function obtained after applying the topology optimization algorithm, but, on the other hand, the thinner the beam, the smaller the objective function. If there are no limits for the length of a desired harvesting device, these results support the production of thinner piezoelectric beam-like structures to maximize the conversion factor.

5.2 Example 4: Substrate thickness percentage β analysis

The effects of another geometric parameter on the objective function and the optimized topology that can be analysed is the substrate's thickness in comparison to the overall thickness of the harvester. Multiple values for β are chosen and the algorithm is run, for a constant total harvester thickness of $H = 40mm$. The other parameters are the same as Example 3. The results are shown in Fig. 7.

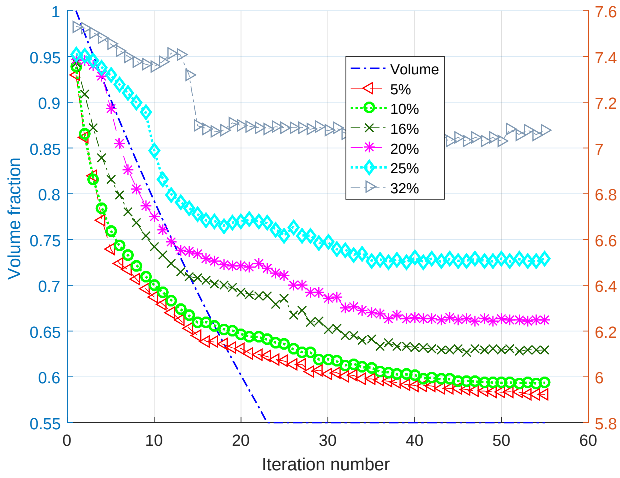

(a) Convergence curve

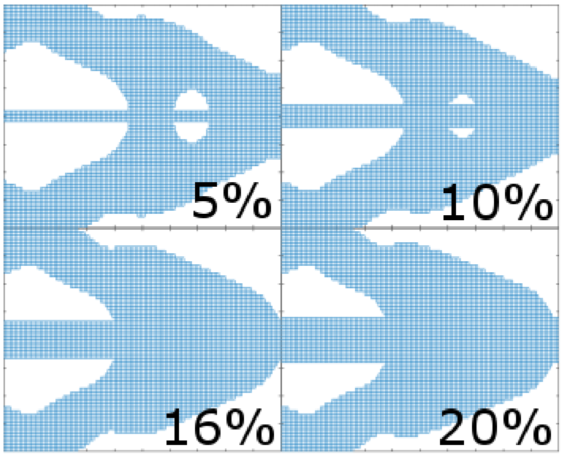

(b) Final topologies for different substrate thickness ratios

Figure 7: Topology optimization results for the piezoelectric harvester with different substrate thickness ratios

As can be seen in Fig. 7a, and through the optimization code, the objective function decreases in 19.1%, 18.8%, 17.0%, 15.5% and 12.0%, corresponding with the substrate thickness ratios shown in Fig. 7a's legend in ascending order. It can be concluded that the thinner the substrate for a fixed beam thickness, the better the conversion factor. This result can be of interest for the manufacturing of piezoelectric harvesters and can be further empirically studied.

6 MATERIALS ANALYSES

In this section, the effects of the energy harvesters' materials on the algorithms convergence and optimal topology are analysed. The penalization factor combination used is $[3, 2, 1]$, with the geometric properties $L = 100mm$, $H = 40mm$ and $\beta = 20\%$.

6.1 Example 5: Substrate material analysis

Firstly, three different substrate materials are analysed - steel plus two new ones: aluminium, with an elastic constant of $68GPa$ and Poisson's coefficient of 0.36; and copper, with the same respective properties of $117GPa$ and 0.33. The rest of the optimization parameters are the same as from Example 1. The piezoelectric material used is PZT-4. The results are displayed in Fig. 8.

In Fig. 8a and through the optimization code we obtain percentile reductions of the objective function of 18.6%, 16.8% and 15.5%, for the harvesters with substrate materials of aluminium, copper and steel, respectively. But, it can also be seen that the final objective function values for the different substrates are very similar to one another. Additionally, from Fig. 8b, the final topologies for the different substrates are almost identical.

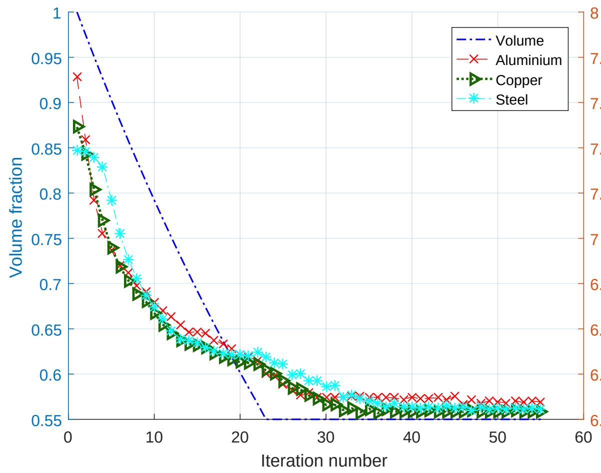

(a) Convergence curve

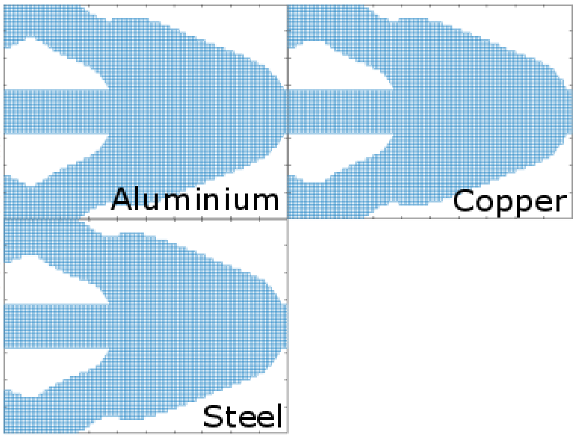

(b) Final topologies for different substrate materials

Figure 8: Topology optimization results for the piezoelectric harvester with different substrate materials

6.2 Example 6: Piezoelectric material analysis

Lastly, three different piezoelectric materials are analysed: PZT-4 and PZT-5A and PZT-5H. Their properties are displayed in Table 1. The substrate material is steel and the other optimization parameters are the same as from Example 1. The results are displayed in Fig. 9.

Table 1: PZT-5A and PZT-5H material properties

Properties	PZT-5A	PZT-5H
$\mathbf{e}\ [C/m^2]$	$\begin{bmatrix} 0 & 0 & -5.36 \\ 0 & 0 & -5.36 \\ 0 & 0 & 15.78 \\ 0 & 12.29 & 0 \\ 12.29 & 0 & 0 \\ 0 & 0 & 0 \end{bmatrix}$	$\begin{bmatrix} 0 & 0 & -6.62 \\ 0 & 0 & -6.62 \\ 0 & 0 & 23.24 \\ 0 & 17.03 & 0 \\ 17.03 & 0 & 0 \\ 0 & 0 & 0 \end{bmatrix}$
$\mathbf{c^E}\ [10^2 GPa]$	$\begin{bmatrix} 1.21 & 0.754 & 0.752 & 0 & 0 & 0 \\ 0.754 & 1.21 & 0.752 & 0 & 0 & 0 \\ 0.752 & 0.752 & 1.11 & 0 & 0 & 0 \\ 0 & 0 & 0 & 0.211 & 0 & 0 \\ 0 & 0 & 0 & 0 & 0.211 & 0 \\ 0 & 0 & 0 & 0 & 0 & 0.226 \end{bmatrix}$	$\begin{bmatrix} 1.27 & 0.802 & 0.847 & 0 & 0 & 0 \\ 0.802 & 1.27 & 0.847 & 0 & 0 & 0 \\ 0.847 & 0.847 & 1.15 & 0 & 0 & 0 \\ 0 & 0 & 0 & 0.230 & 0 & 0 \\ 0 & 0 & 0 & 0 & 0.230 & 0 \\ 0 & 0 & 0 & 0 & 0 & 0.235 \end{bmatrix}$
$\boldsymbol{\varepsilon^S}\ [nF/m]$	$\begin{bmatrix} 8.14 & 0 & 0 \\ 0 & 8.14 & 0 \\ 0 & 0 & 7.32 \end{bmatrix}$	$\begin{bmatrix} 15.1 & 0 & 0 \\ 0 & 15.1 & 0 \\ 0 & 0 & 12.7 \end{bmatrix}$

On one hand, in Fig. 9a and through the optimization code, we obtain percentile reductions of the objective function of 19.3%, 15.5% and 13.8%, for the harvesters with piezoelectric materials of PZT-5H, PZT-4 and PZT-5A, respectively. But, on the other hand, it can be also be seen that the final objective function values for the different materials differ substantially from one another, in comparison to the results when using different substrate materials (from Fig. 8a), with PZT-5A having a 0.6076 better inverse conversion ratio than with PZT-4 and the latter having a 2.53 better conversion ratio than with PZT-5H. From Fig. 9b, the final topologies for the different piezoelectric materials are similar.

From the results displayed in Fig. 8, one can conclude that the topology optimization algorithm can yield better relative results of the objective function for less stiff materials, although

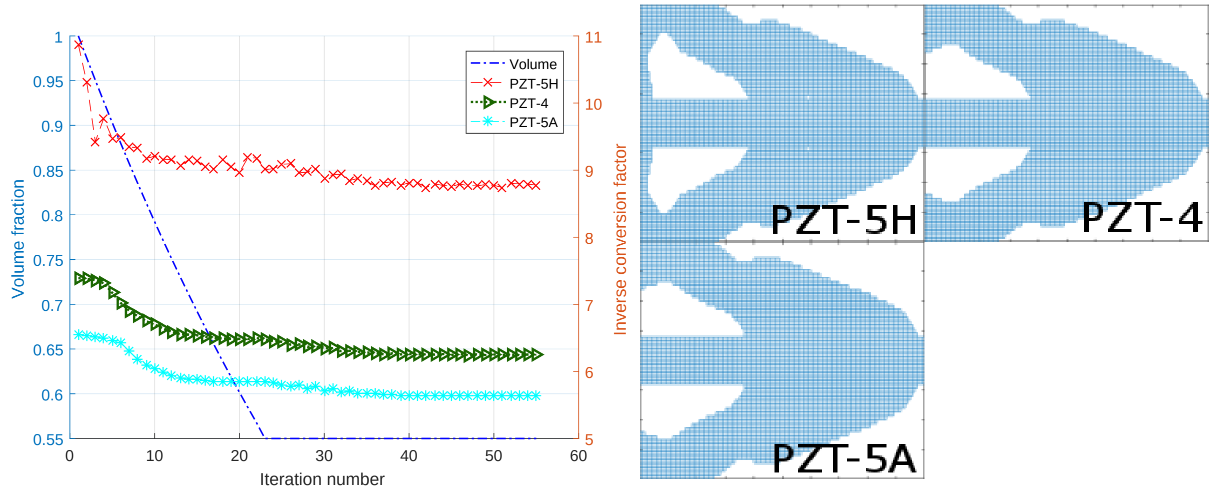

(a) Convergence curve

(b) Final topologies for different piezoelectric materials

Figure 9: Topology optimization results for the piezoelectric harvester with different piezoelectric materials

the final value of the objective function for the different materials might not differ too much from one another in the final topology. Though, from the results displayed in Fig. 9, one can conclude that, in this case, it is more advantageous to use PZT-5A as the piezoelectric material for the harvester, since the inverse conversion factor is the smallest.

7 CONCLUSIONS

A two-dimensional FE model of a bimorph piezoelectric harvester under plain-strain hypothesis was created and the design of the piezoelectric material of the harvester was then structurally optimized using the proposed multiparameter BESO method to minimize the inverse conversion factor. Different penalization factors, one for each physical property of the piezoelectric material, were chosen in order to find a better convergence for the algorithm and the results are shown in Fig. 4. The best combination of penalization factors, considering both the smallest final inverse conversion factor and the optimization convergence stability, was $[3, 2, 1]$.

The topology of the piezoelectric harvester was then optimized considering different geometries: first analysing the effects of the thickness to length ratio for a fixed substrate to piezoelectric thickness ratio, with the results shown in Fig. 6; and then analysing the effects of the latter, while fixing the former, with the results shown in Fig. 7. For the case studies presented, it can be seen that the best geometry would be a harvester composed of two thin piezoelectric layers, for a minimum inverse conversion factor, although the topology optimization algorithm converges best for a thicker geometry, and a intermediate metallic substrate may be necessary for manufacturing reasons. This can be further empirically studied.

Finally, the effects of the substrate material on the inverse conversion factor was studied and its effect on the optimization algorithm, with the results displayed in Fig. 8. The algorithm appears to be more efficient in minimizing the objective function for less stiff materials, although the final topology for the conditions utilized for the convergence resulted in approximately the same final inverse conversion factor and an identical topology for each case. Additionally, the best conversion factors were found for PZT-5A as the piezoelectric material in the harvester.

The results shown in this paper allow for a better understanding of how the topology optimization algorithm for piezoelectric harvesters subjected to a static load using a multiparameter BESO method works, favouring future developments considering harmonic excitations or empirical studies.

ACKNOWLEDGEMENTS

The authors are grateful to FAPESP (São Paulo Research Foundation, grant number 2013/08293-7) and CAPES (Coordination for the Improvement of Higher Education Personnel) for the financial support of this work.

REFERENCES

Azevedo, F., Picelli, R., Vicente, W., & Pavanello, R., 2016. A bi-directional evolutionary topology optimization method applied for acoustic mufflers design. In *5th International Conference on Engineering Optimization*, EngOpt, Iguassu Falls, Brazil.

Bendigeri, R., Tomar, R., S, B., & K, A., 2011. Detailed formulation and programming method for piezoelectric finite element. vol. 7, n. 1, pp. 1–21.

Bendsoe, M. P. & Sigmund, O., 2013. *Topology Optimization: Theory, Methods, and Applications*. Springer-Verlag.

Donoso, A. & Sigmund, O., 2008. Optimization of piezoelectric bimorph actuators with active damping for static and dynamic loads. *Structural and Multidisciplinary Optimization*, vol. 38, n. 2, p. 171.

Dutoit, N. E., Wardle, B. L., & Kim, S.-G., 2005. Design considerations for MEMS-scale piezoelectric mechanical vibration energy harvesters. *Integrated Ferroelectrics*, vol. 71, n. 1, pp. 121–160.

Erturk, A. & Inman, D. J., 2011. *Piezoelectric Energy Harvesting*. John Wiley & Sons, Ltd.

Huang, X. & Xie, M., 2010. *Evolutionary Topology Optimization of Continuum Structures: Methods and Applications*. Wiley.

IEEE, 1988. IEEE Standard on piezoelectricity. *ANSI/IEEE Std 176-1987*.

Kiyono, C. Y., Silva, E. C. N., & Reddy, J. N., 2016. Optimal design of laminated piezocomposite energy harvesting devices considering stress constraints. *International Journal for Numerical Methods in Engineering*, vol. 105, n. 12, pp. 883–914.

Lippmann, G., 1881. Principe de la conservation de l'électricité, ou second principe de la théorie des phénomènes électriques. *Journal de Physique Théorique et Appliquée*, vol. 10, n. 1, pp. 381–394.

Noh, J. Y. & Yoon, G. H., 2012. Topology optimization of piezoelectric energy harvesting devices considering static and harmonic dynamic loads. *Advances in Engineering Software*, vol. 53, pp. 45 – 60.

Picelli, R., Vicente, W. M., Pavanello, R., & Xie, Y. M., 2015. Evolutionary topology optimization for natural frequency maximization problems considering acoustic-structure interaction. *Finite Elements in Analysis and Design*, vol. 106, pp. 56 – 64.

Rajapakse, R., 1997. Plane strain/stress solutions for piezoelectric solids. *Composites Part B: Engineering*, vol. 28, n. 4, pp. 385–396.

Roundy, S. & Wright, P. K., 2004. A piezoelectric vibration based generator for wireless electronics. *Smart Materials and Structures*, vol. 13, n. 5, pp. 1131–1142.

Sigmund, O., Torquato, S., & Aksay, I. A., 1998. On the design of 13 piezocomposites using topology optimization. *Journal of Materials Research*, vol. 13, n. 4, p. 10381048.

Silva, C. E. N., Ono Fonseca, J. S., de Espinosa, F. M., Crumm, A. T., Brady, G. A., Halloran, J. W., & Kikuchi, N., 1999. Design of piezocomposite materials and piezoelectric transducers using topology optimization—part i. *Archives of Computational Methods in Engineering*, vol. 6, n. 2, pp. 117–182.

Sodano, H. A., Park, G., & Inman, D. J., 2004. Estimation of electric charge output for piezoelectric energy harvesting. *Strain*, vol. 40, n. 2, pp. 49–58.

Steven, G. P. & Xie, Y. M., 2014. *Evolutionary Structural Optimization*. Springer.

Vicente, W. M., Picelli, R., Pavanello, R., & Xie, Y. M., 2015. Topology optimization of frequency responses of fluid-structure interaction systems. *Finite Elements in Analysis and Design*, vol. 98, pp. 1–13.

Young W. Kwon, H. B., 2000. *The Finite Element Method Using MATLAB*. Taylor & Francis Inc.

Zheng, B., Chang, C.-J., & Gea, H. C., 2008. Topology optimization of energy harvesting devices using piezoelectric materials. *Structural and Multidisciplinary Optimization*, vol. 38, n. 1, pp. 17–23.